



Mapping vegetation functional types in urban areas with WorldView-2 imagery: Integrating object-based classification with phenology

Jingli Yan^{a,b}, Weiqi Zhou^{a,b,*}, Lijian Han^{a,b}, Yuguo Qian^{a,b}

^a State Key Laboratory of Urban and Regional Ecology, Research Center for Eco-Environmental Sciences, Chinese Academy of Sciences, Beijing 100085, China

^b University of Chinese Academy of Sciences, Beijing 100049, China

ARTICLE INFO

Keywords:

Urban land cover
Vegetation phenology
Vegetation functional type
WorldView-2 imagery
Multi-seasonal images

ABSTRACT

Mapping urban vegetation is a prerequisite to accurately understanding landscape patterns and ecological services provided by urban vegetation. However, the uncertainties in fine-scale vegetation biodiversity mapping still exist in capturing vegetation functional types efficiently at fine scale. To facilitate the application of fine-scale vegetation spatial configuration used for urban landscape planning and ecosystem service valuation, we present an approach integrating object-based classification with vegetation phenology for fine-scale vegetation functional type mapping in compact city of Beijing, China. The phenological information derived from two WorldView-2 imagery scenes, acquired on 14 September 2012 and 26 November 2012, was used to aid in the classification of tree functional types and grass. Then we further compared the approach to that of using only one WorldView imagery. We found WorldView-2 imagery can be successfully applied to map functional types of urban vegetation with its high spatial resolution and relatively high spectral resolution. The application of the vegetation phenology into classification greatly improved the overall accuracy of classification from 82.3% to 91.1%. In particular, the accuracies of vegetation types was improved by from 10% to 13.26%. The approach integrating vegetation phenology with high-resolution remote sensed images provides an efficient tool to incorporate multi-temporal data into fine-scale urban classification.

1. Introduction

Urban ecosystems have been threatened by a deteriorating ecological environment (Bastian et al., 2012) caused by urbanization, particularly in developing countries (Cohen, 2006; Eckert and Kohler, 2014). Meanwhile, urban green infrastructure (GI), particularly trees, can provide numerous ecosystem services (Pickett et al., 2011; Zhou et al., 2017a; Clark et al., 2013; Wu et al., 2013), such as ameliorating air and water pollution (Yan et al., 2016a; Orellana et al., 2012; Jenerette et al., 2011, 2016; Lin et al., 2017); alleviating urban heat islands (Li et al., 2014, 2017; Adams and Smith, 2014; Zhou et al., 2011, 2017b); reducing soil contamination (Boshoff et al., 2014; Curran-Cournane et al., 2015). In addition, these services are highly affected by GI composition and landscape pattern (Li et al., 2013a,b). Therefore, accurately detailed GI mapping is critical to evaluate ecosystem services and to identify vegetation functioning in urban areas (Qian et al., 2015; Zhou and Qiu, 2015).

Remote sensing techniques and products have been widely used for urban vegetation mapping, which is a much more efficient than traditional field investigation (Xie et al., 2008). Some studies began to use

low/medium spatial resolution remote sensed products for vegetation cover mapping (Mucina, 1997; Belward et al., 1990; Running et al., 1995) in last century. However, urban GI is highly heterogeneous and characterized by a large number of small-sized patches, which cannot be detected by low/medium resolution image data (Qian et al., 2015). With the increasing availability of high resolution remote sensed imagery, much more studies have been using high-resolution remote sensed products to achieve higher accuracy for urban greenspace mapping (Mathieu et al., 2007a; Pu et al., 2011; Walker and Blaschke, 2008; Zhou and Troy, 2008).

Recently, increasing attention has been focused on identifying urban vegetation functional types (Mathieu et al., 2007b; Myint et al., 2011; Rapinel et al., 2014; Zhang et al., 2010). These classification accuracy, however, were still relatively low compared to that of urban land cover. Mathieu et al. (2007a) combined IKONOS images and object-based classification to identify large-scale vegetation communities in urban areas of Dunedin city, New Zealand, and the overall accuracy ranged from 63.6% to 77.1%. Even lower accuracies were reported from few studies that attempted to separate tree genera/species with sub-meter resolution (≤ 1 m) remote sensed products. For instance,

* Corresponding author at: Shuangqing Road 18, Haidian District, Beijing 100085, China.
E-mail address: wzhou@rcees.ac.cn (W. Zhou).

Immitzer et al. (2012) found the benefits of additional four spectral information were highly species-dependent when separating European tree species in Austria using a summertime WorldView-2 image. The accuracies ranged from 57% (European hornbeam) to 92% (Lawson's cypress). Pu and Landry (2012) compared the capacity of IKONOS and WorldView-2 for identifying tree species in Tampa, Florida, USA, and found an overall accuracy of WorldView-2 imagery ranging from 65.61% to 67.22% when considering 6-species/group. Up to now, classifying vegetation types or tree species is still a challenge according to existing studies owing to the fragmented GI mosaics and heterogeneous urban environments, as well as shadowed and obscured urban objects (Tigges et al., 2013). In addition, the accuracies of classification were highly depend on the study location, imagery properties, classification approach, and the treatment of shadow (Chasmer et al., 2014; Pu and Landry, 2012; Zhou et al., 2009; Immitzer et al., 2012). Meanwhile, LiDAR data has been applied to some studies as single data source, or integrated with remote sensing images, to utilize its spatial resolution and 3D structure. These studies generally produce higher accuracies than those only deployed remote sensing imagery (Parent et al., 2015; Zhou and Troy, 2008; Li et al., 2013a,b). However, regardless of the spatial misregistration and radiometric differences among different sources of data (Li et al., 2015; Parent et al., 2015; Tooke et al., 2009), the unavailability of LiDAR data in certain places limits its widely applications. Therefore, we need a more accessible and also efficient approach that only using remote sensed products to accurately identify urban vegetation functional types and even tree species in compact cities.

Many previous studies (Aguilar et al., 2013; Hill et al., 2010; Senf et al., 2015; Tigges et al., 2013) suggested that deploying vegetation phenology derived from multi-temporal imagery are helpful to distinguishing the different land covers with a similar phenology trend (Bradley and Mustard, 2008). Vegetation phenology reflects the response of the vegetation to inter- and intra-annual dynamics of the Earth's climate and hydrologic regimes (Myneni et al., 1997; Schwartz and Reed, 1999; White et al., 1997; Richardson et al., 2013; Wu et al., 2013). In most terrestrial ecosystems, forestry canopy processes related to leaf development and senescence are strongly controlled by climate and hydrological conditions (Chuine et al., 2010; Melaas et al., 2013). Phenological dynamics are usually collected using two approaches: surface observation networks (Schwarz et al., 2012), and satellite remote sensing (Reed et al., 2009). Surface observations provide detailed information related to the timing of leaf development and flowering phenology for individual plants, but the use of such data is limited by data availability, the spatial extent of available samples, and biases inherent to used methods in characterizing vegetation phenology (Cleland et al., 2007). Phenology from remote sensing is determined by the seasonal dynamics of vegetation greenness using spectral signals from satellite sensor platforms (Melaas et al., 2013; Wu et al., 2013). A series of vegetation index (VI) have been extensively used in reconstructing phenological transitions for various vegetation functional types (Hmimina et al., 2013; Wu et al., 2013).

However, the widely used remote sensed phenological data source is the Moderate Resolution Imaging Spectroradiometer (MODIS) and AVIRIS (Aguilar et al., 2013; Ganguly et al., 2010; Gonsamo et al., 2012; Hill et al., 2010; Hmimina et al., 2013; Li et al., 2015; Sakamoto et al., 2010; Wolter et al., 1995; Yan et al., 2015a,b; Zhang et al., 2003). Elvidge and Portigal (1990) found dramatic seasonal spectral changes in annual grasslands and smaller spectral changes in evergreen vegetation in a three-date time series of Airborne Visible Infrared Imaging Spectrometer (AVIRIS) data. Merton (1998) demonstrated seasonal changes in the shape of the red edge in a five-image AVIRIS time series of Jasper Ridge. Wolter et al. (1995) used five Landsat TM and MSS images acquired in different months from 1980 to 1992 to classify forest types in northern Wisconsin, US. Senf et al. (2015) compared the capacity of multi-seasonal Landsat TM data and synthetic imagery combined with Landsat and MODIS of classifying four vegetation types.

The results from synthetic images increased about 30% at overall accuracy compared to results only used multi-seasonal images. Therefore, the identification of urban vegetation types that deploying high-resolution multiple temporal images may produce a higher accuracy, because the high-resolution images have huge advantages of represent urban heterogeneity via more detailed geography and abundant spectrum. However, the studies with high-resolution remote sensed images, especially with sub-meter resolution data are rare (Key et al., 2001; Tigges et al., 2013).

In order to test the capacity of vegetation phenology in fine-scale urban vegetation types mapping, this study deployed sub-meter spatial resolution WorldView-2 imagery acquired from multiple seasons to land cover classification in Beijing urban areas. In this study, we identified vegetation functional types through two different classification schemes based on object-based approach using summer-time imagery and two imagery acquired from summer and early winter. We aimed: to assess the capacity of summer-time WorldView-2 imagery for vegetation type mapping using the object-based image analysis; and to examine the improved capacity of vegetation phenology in vegetation type mapping in highly urbanized Beijing city. The study would provide more proofs that vegetation phenology is quite useful in improving urban vegetation identification.

2. Study area and data

2.1. Study area

Beijing is characterized by its rapid urbanization and heterogeneous urban landscape. The percentage cover of vegetation in Beijing city was 47.4% in 2014, with 15.9 square meters of public vegetation per person, however, the vegetation cover is only approximately 33% in urban areas (Beijing Municipal Bureau of Landscape and Forestry, 2014). Beijing belongs to temperate semi-humid continental climate, which facilitates a high diversity of urban vegetation with both species and structure. Meanwhile, the physiological characteristics of vegetation ecosystem are significantly changed among four distinctive seasons. In growing season ranging from late spring to early autumn, the leaves of deciduous and grass are green because the chlorophyll absorb red and blue lights but reflects the green light. When the temperature getting lower in late autumn to early spring, which restricts the formation of chlorophyll, the amount of chlorophyll in leaves reduces but the carotenoid increased. Then the leaves changing to yellow because the carotenoid reflects yellow light and absorb blue and green light. The spectral features derived from remote sensed images change with the changing of plant physiological, but the changes are distinctive among different vegetation functional types. The deciduous trees and grass are significant changed between growing season and non-growing seasons, but the evergreen trees are essentially unchanged. Therefore, the phenological dynamics that represent the changes in spectral observations are useful to classify urban vegetation types.

The study area is a subset of an area of 24 square kilometers ($6 \times 4 \text{ km}^2$) in the northwest of Beijing, China (Fig. 1), where characterized by heterogeneous and fragmented landscape mosaics. The southern section of the subset is composed of dense urban areas, with scattered small vegetation mosaics. In contrast, the northern section is located in the transition region from downtown to suburban, where parks and universities are the predominant land use types. In this area, different types of vegetation are intertwined and fragmented.

2.2. Data preprocessing

The WorldView-2 satellite, launched in 2009 by DigitalGlobe Inc., is the first very high spatial resolution commercial satellite that provides 8 spectral bands. It has a panchromatic band with a spatial resolution of 46 centimeters, and eight multi-spectral bands cover the spectrum from 400 to 1040 nm at the spatial resolution of 1.84 m (Table 1). Each of the

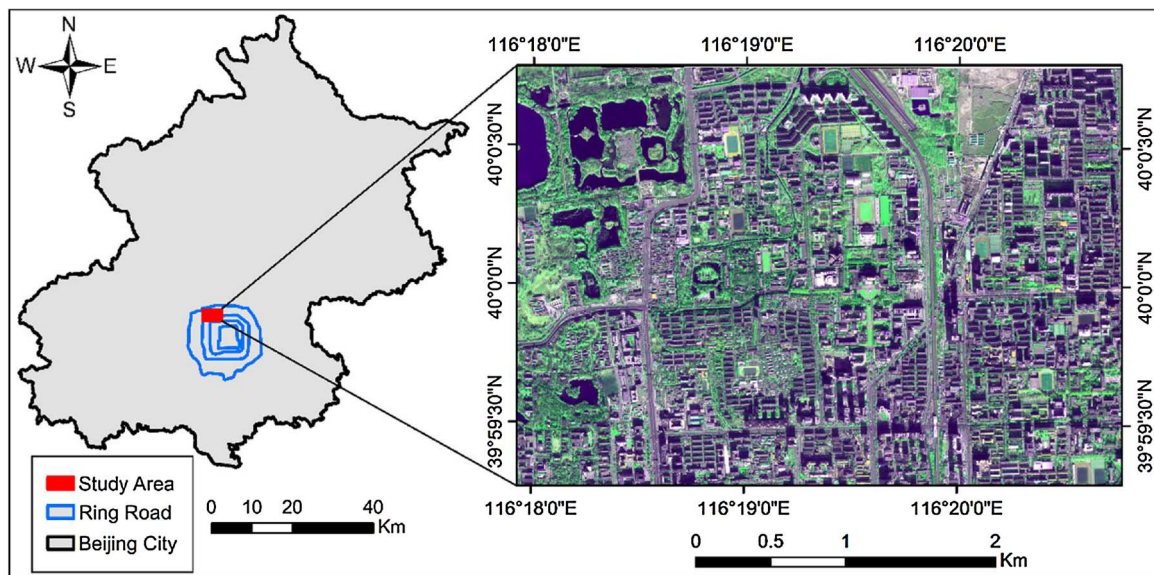


Fig. 1. The study area located between the 3th and 5th ring roads in Beijing, China. The true color combination of WorldView-2 image (26 November, 2012) are Red; Near-Infrared 2; Green.

Table 1
The spectral and spatial information of WorldView-2 imagery.

Spectral band	Wavelength	Spatial resolution
Coastal blue	400–450 nm	1.84 m
Blue	450–510 nm	1.84 m
Green	510–580 nm	1.84 m
Yellow	585–625 nm	1.84 m
Red	630–690 nm	1.84 m
Red-edge	705–745 nm	1.84 m
NIR1	770–895 nm	1.84 m
NIR2	860–1040 nm	1.84 m
Pan	450–800 nm	0.46 m

spectral bands focuses on a particular range of the electromagnetic spectrum that is sensitive to particular features on the ground, or the properties of the atmosphere.

Two scenes of WorldView-2 imagery acquired on September 14, 2012 (IMS) and November 26, 2012 (IMN) respectively were deployed in this classification. They were orthographic calibration-ready standard products obtained under cloudless conditions, and a series of pre-processing steps, including internal sensor geometry correction, removal of optical distortions, scan distortions and line-rate variations, and band registration, were performed by the vendor. Then Gram-Schmidt (GS) algorithm (Padwick et al., 2010) in ENVI 4.8 (<http://www.harrisgeospatial.com/SoftwareTechnology/ENVI.aspx>) was applied to multi-band pan-sharpening because the GS method can produce better spectral quality and maintain the original spectral information of imagery (Yuhendra et al., 2012). Then geometric corrections were conducted in ERDAS IMAGINE™ 2010 (<https://www.hexagongeospatial.com/products/power-portfolio/erdas-imagine>) with controlling the RMS under 0.5. The geocorrection used Google Maps to the same extent as a reference map for two imagery. The referenced Google map was downloaded using Google maps capture software at a spatial resolution of 0.5 m.

3. Vegetation classification

Our study was directed toward two classifications schemes. First we conducted the classification by only using the imagery acquired in September (IMS) (referred to as Method 1). We then examined the classification using multi-seasonal imagery collected from both in

September and November (referred to as Method 2). In Method 2, imagery acquired in November (IMN) was introduced to identify certain vegetation types based on the vegetation phenology. For both methods, the classifications were conducted using object-based procedures (Benz et al., 2004; Blaschke, 2010; Hay et al., 2012) which were implemented in eCognition Developer™ 8.7.

Five classes were included in both classifications-Deciduous Trees (DT), Evergreen Trees (ET), Grass Land (GL), Impervious Surface (IS) and Water Surface (WS). For both classifications, we first applied a multi-resolution segmentation (MRS) algorithm to generate hierarchical image objects. We then separated WS objects from other objects, which were subsequently divided into shaded objects and non-shaded objects. We temporary have shade area because vegetation phenology also can contribute to distinguish vegetation types under shadow. The following procedures for classifying shaded and non-shaded objects were different between two methods, as showed in Figs. 2 and 3.

3.1. Image segmentation

We applied the MRS algorithm embedded in eCognition Developer™ to generate the most appropriate image objects. MRS is a bottom-up segmentation that consecutively merges pixels or existing image objects into bigger objects based on a relative homogeneity criterion (Baatz and Schäpe, 2000; Benz et al., 2004), which measures how homogeneous an image object is within itself. Three key parameters (scale, shape, compactness) can be modified to control homogeneity (Anders et al., 2011). Larger scale parameters result in larger objects, vice versa. If the scale is too larger, the object would mix other land cover types, while too small scale leads to a fragmented landscape (Yan et al., 2016b). The value of shape, which equals 1 minus that of color, determines the weight placed on shape when generating objects. A relatively small value is generally recommended for shape (eCognition Developer reference book; Zhou et al., 2009; Pu and Landry, 2012), so that more weight can be set on color/spectral information. The parameter compactness determines the compactness or smoothness of the objects. Therefore, we set the weights for shape/compactness to 0.2/0.5 in our segmentation according to visual inspection (Baatz and Schäpe, 2000; Benz et al., 2004; Pu and Landry, 2012).

We chose Estimation of Scale Parameter (ESP) (Dragut et al., 2010, 2014) to determine segmentation scale in our study because it is more

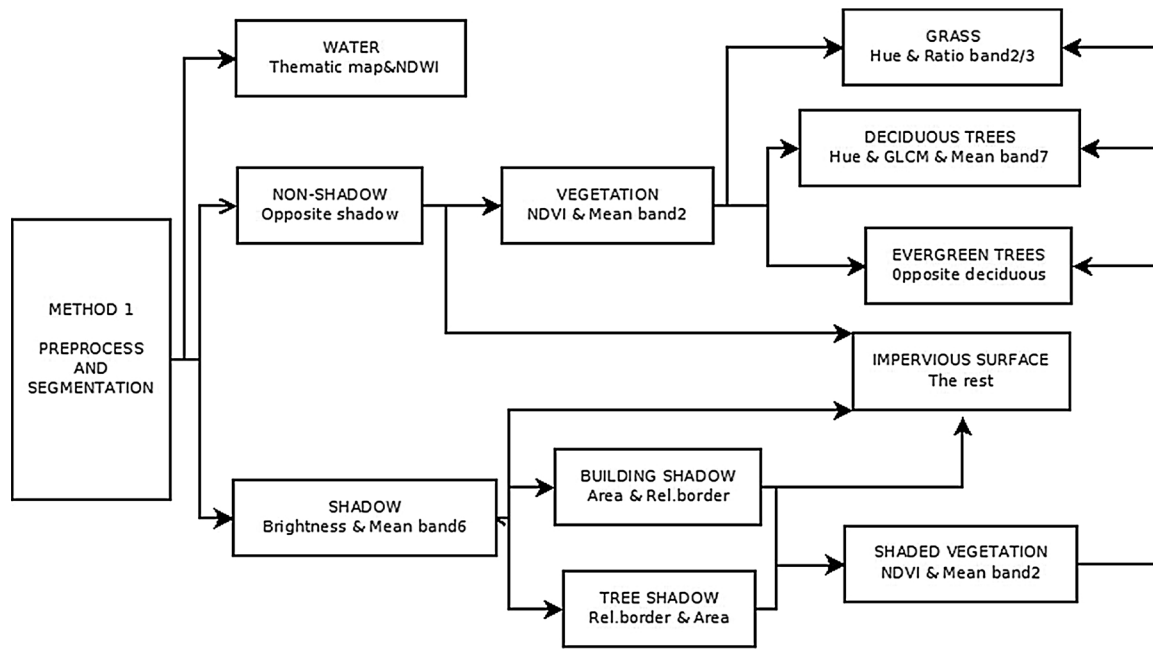


Fig. 2. The classification route map of Method 1. The upper row in the frame is the class name, and the bottom row is the features used for classification.

efficient and subjective compared to visual inspection. The ESP automatically segments the image with fixed increments of scale parameter, and calculates Local Variance (LV) as the mean Standard Deviation (SD) of the objects for each object level obtained through segmentation, and also assesses the dynamics of LV using a measure called Rate of Change (ROC). The peaks in the ROC-LV graph indicate the object levels at which the image can be segmented in the most appropriate manner, relative to data properties at the scene level (Dragut et al., 2010). Results from our ESP analysis indicated there were four optimal scale parameters (30; 50; 75; 95) that may be used for subsequent procedures (Fig. 4). The image segments produced from different scales (Fig. 5) were used to identify corresponding classes, e.g., scale 30 is the best scale for classifying vegetation, while 75 is more appropriate for grass. Therefore, we generated four-level hierarchical object layers using four optimal scale parameters (30, 50, 75, 95 as scale; 0.2/0.5 as shape/compactness) with all eight bands were weighed equally.

3.2. Classification process

3.2.1. Method 1: the classification of only one WV-2 imagery

Method 1 was to test the capacity of classifying vegetation types in urban areas with only one eight-band WV-2 image using the rule-set based classification implemented in eCognition developer™ 8.7. WS objects were first separated using the Normalized Difference Water Index (NDWI) value after segmentation. The image objects with NDWI greater than 0.08 were classified as WS. The remaining unclassified objects were then separated into shaded objects and non-shaded objects using the combinative value of Brightness (25) and Mean Red-edge (170) in membership classification (Table 4). Subsequently, the vegetation in non-shaded objects was identified using the Normalized Difference Vegetation Index (NDVI) values. WV-2 imagery has two Near-infrared bands, in order to fully take the advantage of them, we used both NDVIs ($NDVI1 > 0.365$ and $NDVI2 > 0.35$) simultaneously to improve the accuracy. In addition, the value of Mean blue band

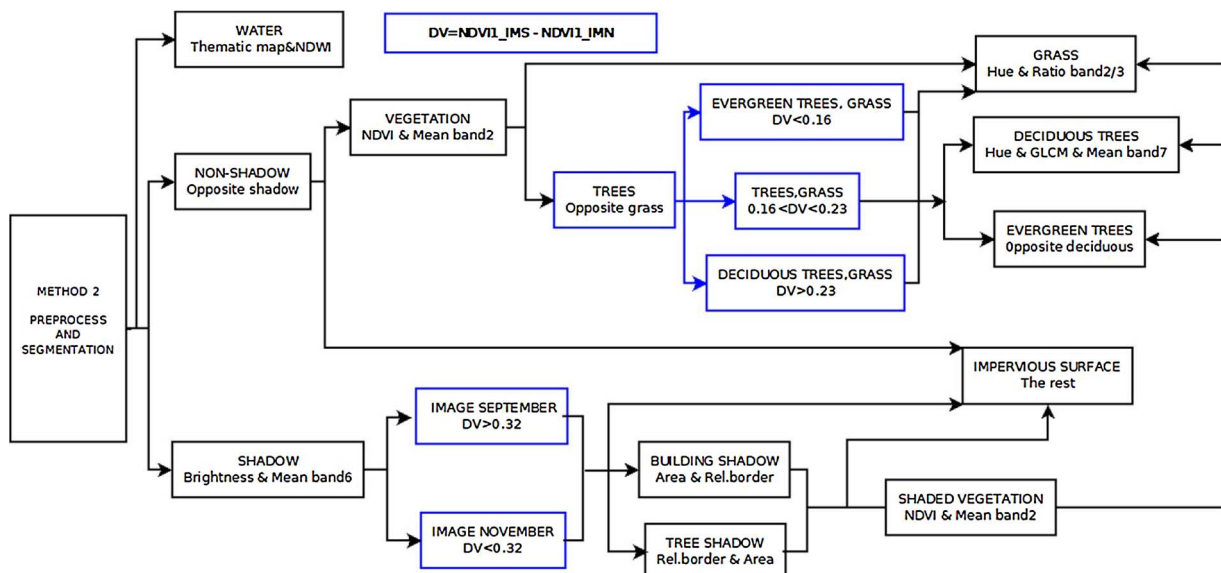


Fig. 3. The classification route map of Method 2. The upper row in the frame is the class name, and the bottom row is the features used for classification.

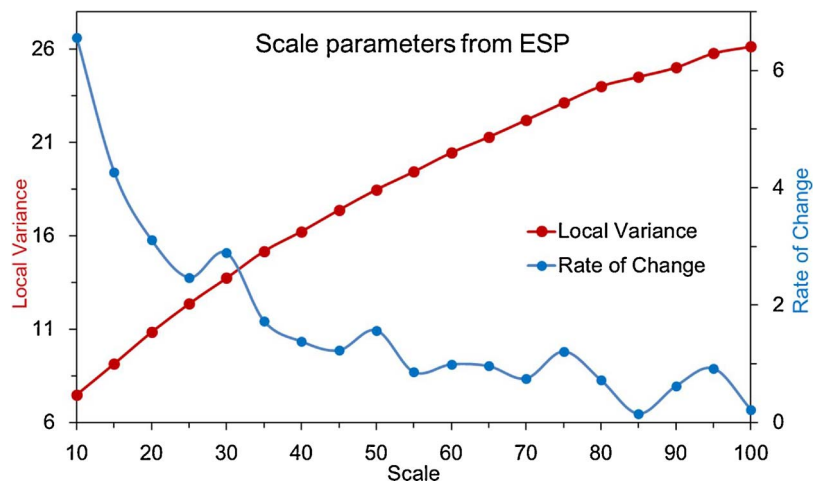


Fig. 4. The optimal scales of segmentation identified by ESP. Scale 30, 50, 75, and 95 were selected for image segmentation.

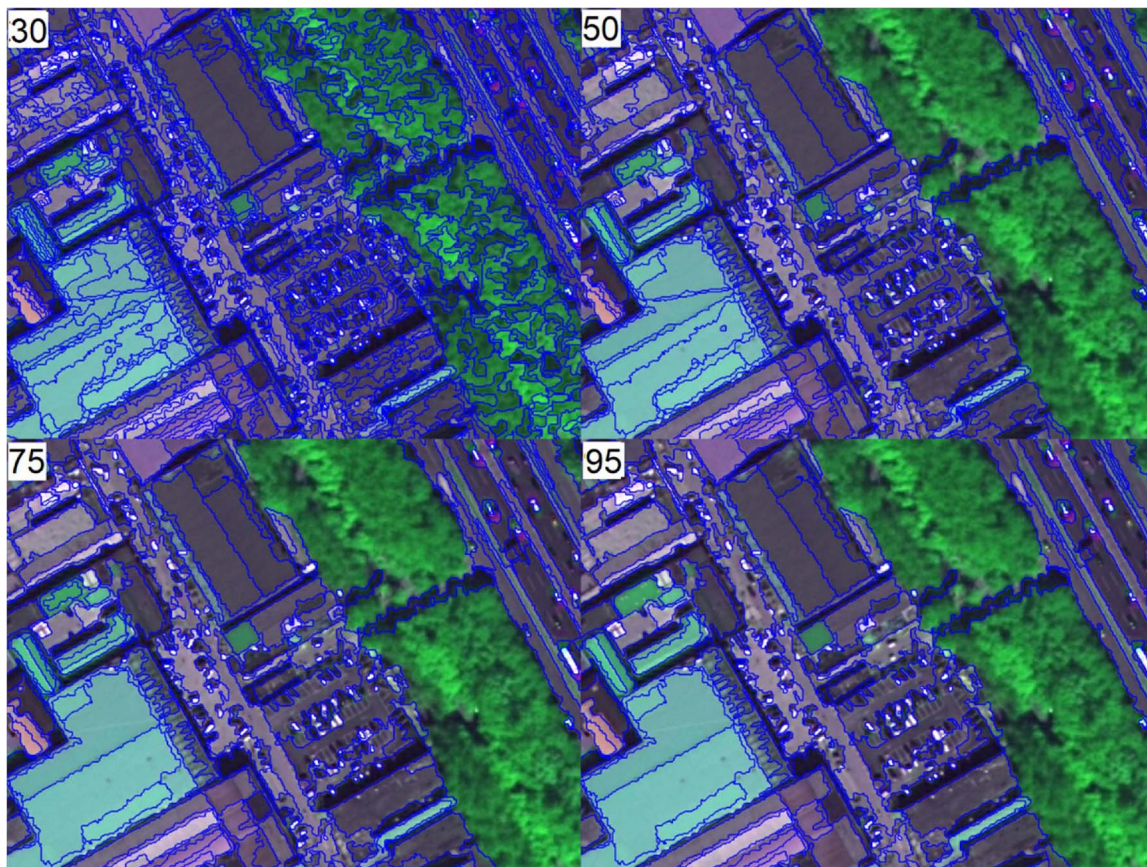


Fig. 5. The segmentation results generated from the four optimal scales suggested by ESP. All scales were used for corresponding classes.

(> 405) was used to remove “colorful roofs” and plastic playgrounds, since their spectral characteristics are similar to vegetation and may be confused with vegetation.

We then divided the non-shaded vegetation into three vegetation types (grasses lands; deciduous trees; evergreen trees) with the selected features resulting from the Classification and Regression Tree (CART). The CART is a non-parametric classification method using training/learning samples to generate accurate and reliable predictive models (Breiman et al., 1984; Laliberte et al., 2012). Three vegetation types were identified by two CART operations: Non-shaded vegetation was first separated into trees and grass in the first operation, deciduous trees and evergreen trees were then separated in the second operation. Before

the CART operation, a total of 1500 training samples (one-third of all collected field samples) were selected, 500 samples for each of deciduous trees, evergreen trees, and grassland. All the samples were randomly selected from 5000 field samples recorded location and tree species/vegetation type. Then all 1500 samples were delineated into shapefile, and input into eCognition developer. In eCognition developer 8.7, we analyzed the similarity between vegetation types at specific features using sample statistic module. Finally, we included 42 features that may be potentially useful for class identification (Table 2) in term of similarity of two vegetation types (similarity index < 0.5). The performance of decision tree in CART mainly determined by two values: Relative Cost (RC) and Rate Of Change (ROC). RC ranges from 0 to 1,

Table 2
The summary of the 42 candidate features used in Classification and Regression Tree.

Feature name	Description
Band 1–8	Means intensity of an image object of bands
Brightness	Mean value of eight bands
SD 1–8	Standard deviations of bands
NDVI 1	(band 7-ban5)/(band 7 + band 5)
NDVI 2	(band 8-ban5)/(band 8 + band 5)
Hue	Means of Hue, one of three color components
Saturation	Means of saturation, one of three color components
Intensity	Means of intensity, one of three color components
Ratio band 2/3	The ratio of band 2 and band3
Ratio band 6/7	The ratio of band 6 and band7
Ratio band 6/8	The ratio of band 6 and band8
Ratio band 7/8	The ratio of band 7 and band8
Elliptic fit	How well an image object fits into an ellipse
Rectangular fit	How well an image object fits into a rectangle
Area	The number of pixels
Compactness	Similar to Border Index, but is based on area
Shape index	The smoothness of an image object border
Border index	How jagged an image object is
Length/width	The ratio of length and width
Length	The length of an image object
Width	The width of an image object
Density	The distribution in space of the pixels of image object
Asymmetry	Describes the relative length of an image object
GLCMH	GLCM homogeneity from band 7 and band 8
GLCMC	GLCM contrast from band 7 and band 8
GLCMD	GLCM dissimilarity from band 7 and band 8
GLCME	GLCM entropy from band 7 and band 8
GLCMA	GLCM angular 2nd moment from band 7 and band 8

with 0 meaning a perfect model, and 1 meaning random guessing. And ROC also ranges from 0 to 1, and higher ROC values suggesting better performance. In addition, more nodes of a decision tree meaning more complexity of rule-set, which increase the difficulty of classification. Considering the performance of CART and the complexity of classification rule-set, a decision tree has 7 terminal nodes with RC of 0.19 and ROC of 0.938 in the first operation, while the tree has 5 terminal nodes with RC of 0.082 and ROC of 0.962 was selected for the second operation. Finally, the features and thresholds that resulted from decision trees were used for establishing rule-sets to separate the three non-shaded vegetation types (Table 3, Fig. 6).

For shaded areas, we separated shadow objects into tree shadow (shadow caused by trees) and building shadow (shadow caused by buildings), because the two types of shadows were too distinct in spectral characteristics to use the same threshold in identifying shaded land covers, e.g., building shadow are generally much darker and bigger than tree shadow. Therefore, the shaded objects with Area greater than 500 pixels (125m²) and Brightness lower than 18 were classified into building shadows, and the rest of the shaded objects were tree shadows. The more boundaries of an object shared with vegetation, the higher possibility of the object belongs to vegetation. Then shaded vegetation was extracted from the two shadow types with combinative use of NDVI2 and Relative border to vegetation (RBV). The RBV was set

Table 3
The summary of the eight most important features resulting from two Classification and Regression Tree operations.

Order	First Operation		Second Operation	
	Feature	Importance	Feature	Importance
1	Ratio band 2/3	100	Hue-RedEdge_NIR1_NIR2	100
2	Hue-Red_Green_Blue	97.33	Ratio band 6/8	97.58
3	Mean Green	85.46	Ratio band 6/7	79.96
4	Mean Yellow	76.61	NDVI2	59.01
5	Brightness	71.18	NDVI1	57.47
6	Mean Red-edge	70.2	Mean NIR2	15.61
7	GLCMH-NIR1	2.4	Mean NIR1	11.22
8	GLCMC-NIR1	2.21	Mean Red-edge	8.61

to 0.5 for two type of shadows, and NDVI2 was set to 0.35 in tree shadow, 0.2 in building shadow. Having shaded vegetation in tree shadow and building shadow, three vegetation types were separated using the same features as in non-shaded vegetation, but the threshold for each feature was different. The remaining unclassified and shaded objects in the entire study area were classified into impervious surface. All classification details were summarized in Table 4.

3.2.2. Method 2: the classification of multi-seasonal WV-2 imagery

Method 2 was developed to examine the advantages of vegetation phenology derived from multi-temporal imagery acquired in September and November for vegetation type classification. Considering the vegetation phenology would improve the accuracies of vegetation classification, we used the IMN as auxiliary data in Method 2 to produce phenological dynamics. Under this approach, phenological differences were applied to identify vegetation types in non-shaded vegetation, and the whole processes in shaded areas. Therefore, the procedures before those steps were exactly the same as in Method 1.

For non-shaded areas, we developed the Phenological Differences (PD) to represent the NDVI difference of the two corresponding image objects at IMS and IMN (PD = NDVI1_IMS-NDVI1_IMN). Then we used PD to separate evergreen trees from deciduous trees following the facts that most leaves of deciduous trees fall in late November which causes the reduction of NDVI value. For non-shaded objects, the objects were classified into evergreen trees if the PD < 0.16, and objects were classified into deciduous trees if the PD > 0.23. If 0.16 < PD < 0.23, those corresponding objects were classified into mixed type of evergreen and deciduous trees, which was further separated into evergreen trees and deciduous trees using the same features used in Method 1.

In shaded areas, PD was used to determine the more appropriate image, on which to conduct the following procedures. If the PD > 0.32, then the following classification procedures were conducted on IMS; otherwise, the IMN was used for the following classifications. Afterwards, tree shadow and building shadow were extracted from shaded areas of two images with the same features used in Method 1. Subsequently, shaded vegetation was identified from two types of shadows only using the values of NDVI2, because NDVI1 is insufficient to detect shaded vegetation. The threshold of NDVI2 on IMS was identical to that of Method 1; but the thresholds for IMN were set to 0.23 in tree shadow and 0.12 in building shadow. Finally, the shaded vegetation was separated into three vegetation types used the same features in Method 1, but different thresholds in Table 4.

3.3. Accuracy assessment

The accuracy assessments were conducted separately for the two methods. For each classified map, we first created a total number of 300 checking points through a stratified random scheme in ERDAS IMAGINE™ 2010, with 60 points for each of the five classes. The collected field samples, except for 1500 training samples used in CART, and google maps were used as the reference data. Some field visits were

Table 4
The summary of features (thresholds) and segmentation scales used in classification for each class.

Class name (Segmentation scale)	Feature (threshold)
Water (95)	NDWI(0.08)
No-shaded areas & Shaded areas (30)	Brightness(25); Mean Red-edge(170)
Tree shadow & Building shadow (95)	Area(500pixels); Relative border to vegetation(0.5)
Vegetation (30)	NDVI1(0.365); NDVI2(0.35); Mean blue(405)
Shaded Vegetation (50)	Tree Shadow NDVI2(0.35 for IMS; 0.23 for IMN); Building Shadow NDVI2(0.2 for IMS; 0.12 for IMN)
Grass/lawns (75) in Non-shaded area	Ratio 2/3(0.82); GLCMH_NIR1(0.05); Hue-Red_Green_Blue(0.44)
Grass/lawns (75) in Shaded area	Ratio 2/3(0.33); GLCMH_NIR1(0.02); Hue-Red_Green_Blue(0.23)
Deciduous Trees & Evergreen Trees (50) in Non-shaded area	Mean NIR2(316.34); Mean RedEdge(350.05); Hue-Edge_NIR1_NIR2(0.32)
Deciduous Trees & Evergreen Trees (50) in Shaded area	Mean NIR2(176.28); Mean RedEdge(102.53); Hue-Edge_NIR1_NIR2(0.14)

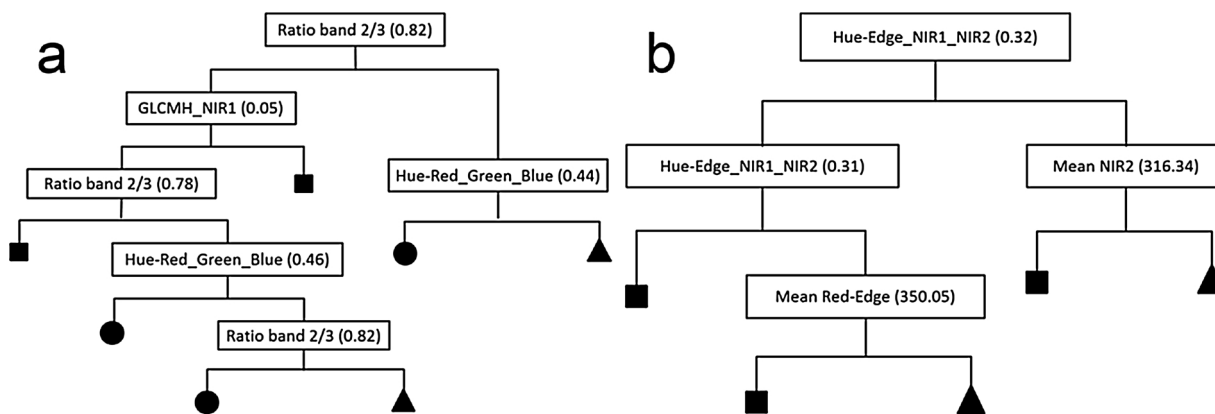


Fig. 6. The resultant decision tree of the two CART operations. Tree A was generated from the first operation, which was used to separate grass; tree B was generated from the second operation to separate deciduous trees. The square means “above average” risk, triangle means “below average” risk, and circle means moderate. The figures in parenthesis are thresholds, and the high values are on the right.

also finished if necessary, e.g., the locations were not only excluded from our field samples, but have uncertainties in identify them just based on google maps. Then confusion matrixes were generated to calculate the overall accuracy (OA), user’s accuracy (UA) and producer’s accuracy (PA), and Kappa coefficient (KC) for each method. Finally, we compared the accuracy changes between two classification schemes.

4. Results

With Method 1, the overall accuracy of classification was 82.3%, and the Kappa coefficient was 0.811 (Fig. 7a, Table 5). The user’s accuracy ranged from 73.33% of ET to 93.33% of the WS, while producer’s accuracy ranging from 67.69% of ET to 94.96% of WS (Table 5). The ET and WS always had the lowest and highest accuracy in two kinds of accuracies. The confusion matrix showed that misclassifications mainly occurred among vegetation types, as well as between vegetation types and IS. 10 of the 11 misclassified DTs were mostly misclassified into ETs (8 of 11) or GLs (2 of 11). Similarly, 12 out of the 16 misclassified ETs were misclassified into DT (7 of 16) and GLLs (5 of 16). And 11 of 15 misclassified GLs were mistaken to tree types.

With Method 2, the overall accuracy and Kappa coefficient increased to 91.1% and 0.881, respectively (Fig. 7b, Table 6). Similar to Method 1, ET had the lowest accuracy, and WS had the highest accuracy. The overall accuracy had been improved, but the misclassifications among vegetation types still the major errors. Most of the misclassified DT were confused with ET (4 of 5), and the misclassified ET equally spread to all the other classes. For method 2, GL had more opportunities of misclassifying to ET (5 of 7).

The overall accuracy of Method 2 with vegetation phenology used in classification was improved by 8.8%, and the user’s accuracies of classes were increased for all classes ranging from 3.33% of WS to 11.67% of ET and GL. In particular, the three vegetation types were

benefited most from vegetation phenology dynamics, ranging from 10% to 11.67% with an average increase of 11.1% for user’s accuracy, even higher for producer’s accuracy (Table 7).

5. Discussion

5.1. The utilization of vegetation phenology can significantly improve the accuracy urban vegetation classification

The results showed that integrating vegetation phenology derived from multi-seasonal images with high-resolution remote sensed products could significantly improve classification accuracy, which is consistent with previous studies using low- and moderate-resolution images (Hill et al., 2010; Senf et al., 2015; Tigges et al., 2013; Ganguly et al., 2010; Gonsamo et al., 2012; Hill et al., 2010; Hmimina et al., 2013). The overall accuracy of Method 2, which deployed phenological information into the classification, increased by 8.8% from 82.3% of Method 1–91.1% of Method 2. In particular, the user’s accuracies for the three vegetation classes were greatly improved by from 10% to 11.67%. The accuracy improvements of DT and GL were mainly resulted from vegetation phenology. In the winter, only few leaves left on deciduous trees or trees have been changed its color, and the grass is declining, so the plants reflect yellow light because the reduction of chlorophyll and the increase of carotenoid. Then the changes of spectral characteristics leading to the changes of NDVI, so we can identify those vegetation types according to the NDVI differences among multiple seasons. In addition to phenological dynamics, the abundant spectral information, the fine scale geographical details, and also the transparency and size of shadow in different seasons were the important advantages to the separation of vegetation types.

It should be noted that the ancillary imagery of Method 2 was acquired in late November. In Beijing, the leaves usually began to fall at mid of October, while the deciduous species still have few leaves left on

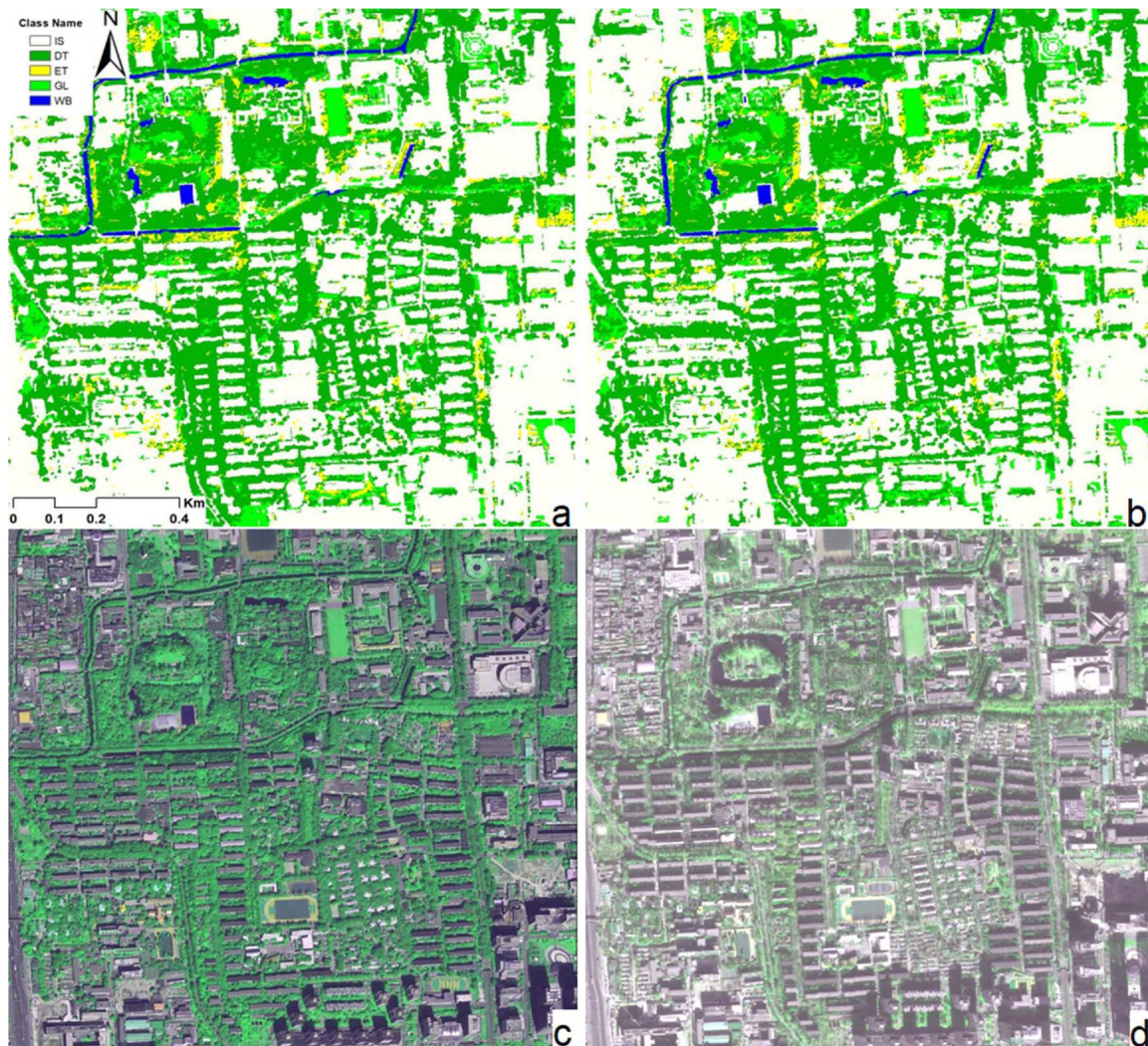


Fig. 7. The classification results of a subset of the study area, panel a-the classification obtained from Method 1; panel b-the classification from Method 2; panel c-the subset of the original imagery corresponding to panel a; panel d-the subset of the original imagery corresponding to panel b.

Table 5
The confusion matrix, accuracies, and Kappa coefficients for Method 1.

Classified	Reference					Total	UA(%)
	DT	ET	GL	IS	WS		
DT	49	8	2	1	0	60	81.67
ET	7	44	5	2	2	60	73.33
GL	5	6	46	2	1	60	76.67
IS	2	4	2	52	0	60	86.67
WS	0	3	1	0	56	60	93.33
Total	63	65	56	57	59	300	
PA(%)	77.78	67.69	82.14	91.23	94.92		

Overall Accuracy = 82.3%; Kappa Coefficient = 0.811.

the trees, and grass is deteriorated but nor ruined. In addition, the vegetation mosaics in study area are intertwined, and the boundaries between them are very difficult to accurately delineate. Such disadvantages restrict the better performance of phenological dynamics. Therefore, greater improvement of classification accuracies can be expected if the imagery was collected on a better date (e.g., January).

Table 6
The confusion matrix, accuracies, and Kappa coefficients for Method 2.

Classified	Reference					Total	UA(%)
	DT	ET	GL	IS	WS		
DT	55	4	1	0	0	60	91.67
ET	3	51	2	2	2	60	85
GL	2	5	53	0	0	60	88.33
IS	1	3	0	56	0	60	95
WS	1	0	1	1	57	60	96.67
Total	62	63	57	59	59	300	
PA(%)	88.71	80.95	92.98	95	98.31		

Overall Accuracy = 91.1%; Kappa Coefficient = 0.881.

5.2. WorldView-2 imagery can be effectively used to map vegetation functional types in compact urban areas

The comparison between our results and other existing ones from similar studies related to urban vegetation classification indicates that the accuracies resulted from the Method 2 of our study are relatively high (Table 8). The overall accuracies of previous studies ranged from 44.06% to 97.58% in term of different data and methods. The studies have achieved the overall accuracy higher than 90% (similar to that of Method 2) either integrated LiDAR with other remote sensed data

Table 7
The changes in accuracy between the two classifications, CE = Commission Error; OE = Omission Error.

Class Name	Change in percentage (Method 2-Method 1;%)			
	PA	UA	CE	OE
DT	10.93	10	-10	-10.93
ET	13.26	11.67	-11.67	-13.26
GL	10.84	11.67	-11.67	-10.84
IS	5.38	8.33	-8.33	-5.38
WS	3.39	3.33	-3.33	-3.39
Average	9%	8.76%	-8.76%	-9%

(Tigges et al., 2013; Parent et al., 2015; Zhou and Qiu, 2015) or identified fewer vegetation types (Sridharan and Qiu, 2013; Myint et al., 2011) than this study. According to previous studies, LiDAR is a quite useful in identifying of vegetation functional types, even tree species, especially when integrating LiDAR with high-resolution remote sensed images (Alonzo et al., 2014; Li et al., 2013a,b; Yan et al., 2015a, 2015b; Zhou et al., 2009). However, to this day, the limitations in availability of LiDAR, and spatial misregistration and radiometric differences

among different data sources, are all restrict the intensive use of LiDAR (Dare, 2005).

With a single scene of WorldView-2 imagery, the Method 1 obtained an overall accuracy of 82.3%, with user's accuracy ranged from 73.33% to 93.33% for five classes. These accuracies were generally higher than or equal to those of studies used single time high spatial resolution imagery (Mallinis et al., 2008; May et al., 1997; Parent et al., 2015), and also are comparable to those from studies using multiple-source data (Hill et al., 2010; Tooke et al., 2009; Senf et al., 2015). According to our results, WorldView-2 imagery could be effectively used to map vegetation functional types in urban areas, which is consistent with studies of Chen, 2010 and Pu and Landry, 2012. With a sub-meter spatial resolution of 0.46 m, WorldView-2 imagery can sufficiently discriminate fine-scale land covers and tree crowns, as well as shadows in heterogeneous urban environments. In Addition, WorldView-2 imagery owns 8 multi-spectral bands in contrast to most high spatial resolution images only has 4 bands. The 8 spectral bands, covering the wavelength of 400–1040 nm, are sensitive to particular features, and provide more accurate spectral information for geographic features in diverse urban environments. The four new additional bands (Coastal blue, Yellow, Red-edge, and NIR2) enable the images to present the

Table 8
A list of case studies that focused on vegetation classification.

Case study	Study area	Data	Methods/ Analytical unit	Total classes & Vegetation classes	Overall Accuracy
Li et al. (2015)	Beijing, China	WorldView-2 WorldView-3	SVM, RF/ OB	4 Tree species	71–82.7% for WV-2 70–76.3% for WV-3 80.3–92.4% for Both
Zhou and Qiu (2015)	Dallas, USA	WorldView-2 LiDAR	KL/ OB	5 classes & Trees, grass	89.97% WV-2 only; 97.58% multi-data
Parent et al. (2015)	Northeastern USA	Aerial Image LiDAR	Ruleset/ PB, OB	5 or 8 classes & Deciduous, coniferous, medium vegetation, low vegetation	93.1% for 8 classes 94.8% for 5 classes
Senf et al. (2015)	Southern Portugal	Multi-Temporal Landsat TM, MODIS	SVM/ OB	5 classes & Wood, shrub, grass	44.06%–74.49%
Puissant et al. (2014)	Strasbourg, France	QuickBird	RF/ OB	9 classes & Artificial greenspace, Agricultural land	59.08%–98.65%
Sridharan and Qiu (2013)	Dallas, USA	WorldView-2	FKS,NN, SVM/ OB	6 classes & Tree, grass	67.98%–90.51%
Tigges et al. (2013)	Berlin, Germany	Multi-temporal RapidEye, LiDAR	SVM/ PB	8 tree genera	63–100%
Li et al. (2013a)	Sault Ste. Marie, Canada	LiDAR	Supervised classification	4 tree species	74.3–81%
Liu and Yang (2013)	Atlanta, USA	Landsat TM	MLC, SMA/ PB	10 classes & Broad-leaf, needle-leaf, pasture, grass, cropland, vegetation wetland	69.84–81.63%
Duro et al. (2012)	Saskatchewan, Canada	SPOT-5	RF, SVM, DT/ PB, OB	6class& Crop, mixed grassland	87.6–89.7% pixel-based 88.8–94.2% object-based
Al-Kofahi et al. (2012)	Albuquerque, USA	Aerial Image	ENVI EX/ OB	4 classes & Trees, shrub, grass	89%
Pu and Landry (2012)	Tampa, USA	WorldView-2, IKONOS	CART, LDA OB	6 tree species	47.2–67.22%
Myint et al. (2011)	Phoenix, USA	QuickBird	NN,MF PB OB	7 classes & Tree/shrub, grass	67.6% pixel-based 90.4% object-based
Zhang et al. (2010)	Nanjing, China	IKONOS	MLC, CART/ OB	5 classes & Broadleaf, needle-leaf, weed	75.43%–89.42%
Hill et al. (2010)	Cambridgeshire, UK	Multi-temporal ATM images	MLC/ PB	6 tree species	35.4–83.8%
Tooke et al. (2009)	Vancouver, Canada	QuickBird LiDAR	SMA, DT/ PB, OB	6 class & Broad-leaf, needle-leaf, vegetated ground cover	67–80%
Mathieu et al. (2007a)	Dunedin, New Zealand	IKONOS	NN OB	10 or 15 classes & Tree, shrub, grass	63.6% 15 classes 77.1% 10 classes

Note: OB = Object-based; PB = Pixel-based; KL = Kullback–Leibler (KL) divergence based classifier; SVM = Support vector machine; RF = Random Forest; EX = Feature Extraction Module; FKS = Fuzzy Kolmogorov-Smirnov Classifier; SMA = Spectral mixture analysis; NN = Nearest neighbor classifier; MF = Membership functional classifier; MLC = Maximum likelihood classification; DT = Decision tree; CART = Classification and regression tree.

urban objects as what the human eye perceives (DigitalGlobe, 2009). For example, Red-edge and NIR2 bands enhanced the high reflectivity portion of vegetation response (Li et al., 2015), and are critical to identifying tree types in our study.

The comparison of existing studies emphasized the advantages of high-resolution images. Therefore, the question of how many scenes of multi-temporal imagery should be used in a classification to obtain a reasonable accuracy is needed to be answered. While many studies used high frequency low-resolution imagery throughout a year, even longer term, to achieved reasonable accuracies, our study suggested that few high-resolution multi-temporal imagery also can achieve the similar accuracies. Therefore, more studies of recognizing relationships between the number of multi-temporal data used in a classification and the accuracy resulted from the classification are helpful to address the capacity of phenology dynamics in discriminate different vegetation types.

6. Conclusions

The mapping of vegetation types at fine scale is a promotion of ecosystem service valuation, as well as urban GI arrangement. In this study, the capacity of single WV-2 imagery and the vegetation phenology derived from multi-temporal imagery were tested and evaluated in identifying vegetation functional types in compact Beijing city. Classification with single WV-2 imagery achieved an overall accuracy of 82.3%, which indicates that WV-2 imagery is capable of classifying vegetation functional types in a fragmented landscape. The Red-edge and NIR2 band contributed more than traditional bands in identifying vegetation types. The overall accuracy of classification deployed vegetation phenology increased by 8.8% in contrast to classification only using one WV-2 image, and the increase of accuracies of three vegetation type ranged from 10% to 13.26%. Therefore, considering the accuracy, integrating vegetation phenology with few high-resolution multi-temporal remote sensed images is an efficient way to improve urban vegetation classification comparing with using more high frequency lower-resolution multi-temporal images.

Acknowledgements

The research was supported by National Science Foundation of China (Grant No. 41422104; 41771203) and Chinese Academy of Sciences (Grant No. QYZDB-SSW-DQC034). We thank Pengfei Zhao for contributing to the sample collection in the field, and also appreciate the helpful comments from two anonymous reviews.

References

- Adams, M.P., Smith, P.L., 2014. A systematic approach to model the influence of the type and density of vegetation cover on urban heat using remote sensing. *Landscape Urban Plan.* 132, 47–54.
- Aguilar, M.A., Saldana, M.M., Aguilar, F.J., 2013. GeoEye-1 and WorldView-2 pan-sharpened imagery for object-based classification in urban environments. *Int. J. Remote Sens.* 34, 2583–2606.
- Alonzo, M., Bookhagen, B., Roberts, D.A., 2014. Urban tree species mapping using hyperspectral and lidar data fusion. *Remote Sens. Environ.* 148, 70–83.
- Anders, N.S., Seijmonsbergen, A.C., Bouten, W., 2011. Segmentation optimization and stratified object-based analysis for semi-automated geomorphological mapping. *Remote Sens. Environ.* 115, 2976–2985.
- Al-Kofahi, S., Steele, C., VanLeeuwen, D., St Hilaire, R., 2012. Mapping land cover in urban residential landscapes using very high spatial resolution aerial photographs. *Urban For. Urban Green.* 11 (3), 291–301.
- Baatz, M., Schäpe, A., 2000. Multiresolution segmentation—an optimization approach for high quality multi-scale image segmentation. In: Strobl, J., Blaschke, T., Griesebner, G. (Eds.), *Angew. Geogr. Info. Verarbeitung*. Wichmann-Verlag, Heidelberg, pp. 12–23.
- Bastian, O., Haase, D., Grunewald, K., 2012. Ecosystem properties, potentials and services – the EPPS conceptual framework and an urban application example. *Ecol. Indic.* 21, 7–16.
- Belward, A.S., Taylor, J.C., Stuttard, M.J., Bignal, E., Mathews, J., Curtis, D., 1990. An unsupervised approach to the classification of seminatural vegetation from Landsat Thematic Mapper Data – a pilot-study on Islay. *Int. J. Remote Sens.* 11, 429–445.
- Benz, U.C., Hofmann, P., Willhauck, G., Lingenfelder, I., Heynen, M., 2004. Multiresolution, object-oriented fuzzy analysis of remote sensing data for GIS-ready information. *ISPRS J. Photogramm. Remote Sens.* 58, 239–258.
- Blaschke, T., 2010. Object based image analysis for remote sensing. *ISPRS J. Photogramm. Remote Sens.* 65, 2–16.
- Boshoff, M., De Jonge, M., Scheifler, R., Bervoets, L., 2014. Predicting As, Cd, Cu, Pb and Zn levels in grasses (*Agrostis* sp and *Poa* sp.) and stinging nettle (*Urtica dioica*) applying soil-plant transfer models. *Sci. Total Environ.* 493, 862–871.
- Bradley, B.A., Mustard, F., 2008. Comparison of phenology trends land cover class: a case study in the Great Basin, USA. *Glob. Change Biol.* 14, 334–346.
- Breiman, L., Friedman, J.H., Olshen, R.A., Stone, C.J., 1984. *Classification and Regression Trees*. Wadsworth International Group, Belmont, CA.
- Chasmer, L., Hopkinson, C., Veness, T., Quinton, W., Baltzer, J., 2014. A decision-tree classification for low-lying complex land cover types within the zone of discontinuous permafrost. *Remote Sens. Environ.* 143, 73–84.
- Chen, Q., 2010. Comparison of WorldView-2 and IKONOS-2 imagery for identifying tree species in the habitat of an endangered bird species in Hawaii, http://dgl.us.neolane.net/res/dgl/survey/8bandchallenge_researchPapers.jsp.
- Chuine, I., Morin, X., Bugmann, H., 2010. Warming photoperiods, and tree phenology. *Science* 329, 277–278.
- Clark, L.W., Jenerette, G., Davila, A., 2013. The luxury of vegetation and the legacy of tree biodiversity in Los Angeles, CA. *Landscape Urban Plan.* 116, 48–59.
- Cleland, E.E., Chuine, I., Menzel, A., Mooney, H.A., Schwartz, M.D., 2007. Shifting plant phenology in response to global change. *Trends Ecol. Evol.* 22, 357–365.
- Cohen, B., 2006. Urbanization in developing countries: current trends, future projections, and key challenges for sustainability. *Technol. Soc.* 28, 63–80.
- Curran-Cournane, F., Lear, G., Schwendenmann, L., Khin, J., 2015. Heavy metal soil pollution is influenced by the location of green spaces within urban settings. *Soil Res.* 53, 306–315.
- Dare, P.M., 2005. Shadow analysis in high-resolution satellite imagery of urban areas. *Photogramm. Eng. Remote Sens.* 71, 169–177.
- DigitalGlobe, 2009. The benefits of the 8 spectral bands of WorldView-2. <http://worldview-2.digitalglobe.com/>.
- Dragut, L., Tiede, D., Levick, S.R., 2010. ESP: a tool to estimate scale parameter for multiresolution image segmentation of remotely sensed data. *Int. J. Geo. Inf. Sci.* 24, 859–871.
- Dragut, L., Csillik, O., Eisank, C., Tiede, D., 2014. Automated parameterisation for multi-scale image segmentation on multiple layers. *ISPRS J. Photogramm. Remote Sens.* 88, 119–127.
- Duro, D.C., Franklin, S.E., Dube, M.G., 2012. A comparison of pixel-based and object-based image analysis with selected machine learning algorithms for the classification of agricultural landscapes using SPOT-5 HRG imagery. *Remote Sens. Environ.* 118, 259–272.
- Eckert, S., Kohler, S., 2014. Urbanization and health in developing countries: a systematic review. *World Health Popul.* 15, 7–20.
- eCognition Developer reference book, 2011. Trimble Inc. <http://www.ecognition.com/suite/ecognition-developer>.
- Elvidge, C.D., Portigal, F.P., 1990. Change detection in vegetation using 1989. AVIRIS data. *SPIE Int. Soc. Opt. Eng.* 1298, 178–189.
- Ganguly, S., Friedl, M.A., Tan, B., Zhang, X., Verma, M., 2010. Land surface phenology from MODIS: characterization of the collection 5 global land cover dynamics product. *Remote Sens. Environ.* 114, 1805–1816.
- Gonsamo, A., Chen, J.M., Price, D.T., Kurz, W.A., Wu, C., 2012. Land surface phenology from optical satellite measurement and CO2 eddy covariance technique. *J. Geophys. Res.: Biogeosci.* 117.
- Hay, G.J., Blaschke, T., Marceau, D.J., Bouchard, A., 2012. A comparison of three image-object methods for the multiscale analysis of landscape structure. *ISPRS J. Photogramm. Remote Sens.* 57, 327–345.
- Hill, R.A., Wilson, A.K., George, M., Hinsley, S.A., 2010. Mapping tree species in temperate deciduous woodland using time-series multi-spectral data. *Appl. Veg. Sci.* 13, 86–99.
- Hmimina, G., Dufrene, E., Pontailleur, J.Y., Delpierre, N., Aubinet, M., Caquet, B., De Grandcourt, A., Burban, B., Flechard, C., Granier, A., 2013. Evaluation of the potential of MODIS satellite data to predict vegetation phenology in different biomes: an investigation using ground-based NDVI measurements. *Remote Sens. Environ.* 132, 145–158.
- Immitzer, M., Atzberger, C., Koukal, T., 2012. Tree species classification with random forest using very high spatial resolution 8-band WorldView-2 satellite data. *Remote Sens.* 4, 2661–2693.
- Jenerette, G.D., Harlan, S.L., Stefanov, W.L., Martin, C.A., 2011. Ecosystem services and urban heat riskscape moderation: water, green spaces, and social inequality in Phoenix, USA. *Ecol. Appl.* 21, 2637–2651.
- Jenerette, G.D., Harlan, S.L., Buyantuev, A., Stefanov, W.L., Delet-Barreto, J., Ruddell, B.L., Myint, S.W., Kaplan, S., Li, X., 2016. Micro-scale urban surface temperatures are related to land-cover features and residential heat related health impacts in Phoenix, AZ USA. *Landscape Ecol.* 31, 745–760.
- Key, T., Warner, T.A., McGraw, J.B., Fajvan, M.A., 2001. A comparison of multispectral and multitemporal information in high spatial resolution imagery for classification of individual tree species in a temperate hardwood forest. *Remote Sens. Environ.* 75, 100–112.
- Laliberte, A.S., Browning, D.M., Rango, A., 2012. A comparison of three feature selection methods for object-based classification of sub-decimeter resolution UltraCam-L imagery. *Int. J. Appl. Earth Observ. Geoinform.* 15, 70–78.
- Li, J., Hu, B., Noland, T.L., 2013a. Classification of tree species based on structural features derived from high density LiDAR data. *Agric. Forest Meteorol.* 171, 104–114.
- Li, X., Zhou, W., Ouyang, Z., Xu, W., Zheng, H., 2013b. Spatial pattern of greenspace

- affects land surface temperature: evidence from the heavily urbanized Beijing metropolitan area, China. *Landscape Ecol.* 6, 887–898.
- Li, X., Myint, S.W., Zhang, Y., Galletti, C., Zhang, X., Turner, B.L., 2014. Object-based land-cover classification for metropolitan Phoenix, Arizona, using aerial photography. *Int. J. Appl. Earth Observ. Geoinform.* 33, 321–330.
- Li, D., Ke, Y., Gong, H., Li, X., 2015. Object-Based urban tree species classification using Bi-Temporal WorldView-2 and WorldView-3 images. *Remote Sens.* 7, 16917–16937.
- Li, X., Kamarianakis, Y., Ouyang, Y., Turner II, B.L., Brazel, A., 2017. On the association between land system architecture and land surface temperatures: evidence from a Desert Metropolitan-Phoenix, Arizona, USA. *Landscape Urban Plan.* 163, 107–120.
- Lin, L., Yan, J., Ma, K., Zhou, W., Chen, G., Tang, R., Zhang, Y., 2017. Characterization of particulate matter deposited on urban tree foliage: a landscape analysis approach. *Atmos. Environ.* 171, 59–69.
- Liu, T., Yang, X., 2013. Mapping vegetation in an urban area with stratified classification and multiple endmember spectral mixture analysis. *Remote Sens. Environ.* 133, 251–264.
- Mallinis, G., Koutsias, N., Tsakiri-Strati, M., Karteris, M., 2008. Object-based classification using Quickbird imagery for delineating forest vegetation polygons in a Mediterranean test site. *ISPRS J. Photogramm. Remote Sens.* 63, 237–250.
- Mathieu, R., Aryal, J., Chong, A.K., 2013. Object-based classification of ikonos imagery for mapping large-scale vegetation communities in urban areas. *Sensors* 7, 2860–2880.
- Mathieu, R., Freeman, C., Aryal, J., 2007b. Mapping private gardens in urban areas using object-oriented techniques and very high-resolution satellite imagery. *Landscape Urban Plan.* 81, 179–192.
- May, A.M.B., Pinder, J.E., Kroh, G.C., 1997. A comparison of Landsat Thematic Mapper and SPOT multi-spectral imagery for the classification of shrub and meadow vegetation in northern California, USA. *Int. J. Remote Sens.* 18, 3719–3728.
- Melaas, E.K., Friedl, M.A., Zhu, Z., 2013. Detecting interannual variation in deciduous broadleaf forest phenology using Landsat TM/ETM+ data. *Remote Sens. Environ.* 132, 176–185.
- Merton, R.N., 1998. Monitoring community hysteresis using spectral shift analysis and the red-edge vegetation stress index. In: *Proceedings of the Seventh JPL Airborne Earth Science Workshop*. Jet Propulsion Laboratory, Pasadena, CA. pp. 275–284.
- Mucina, L., 1997. Classification of vegetation: past, present and future. *J. Veg. Sci.* 6, 751–760.
- Myint, S.W., Gober, P., Brazel, A., Grossman-Clarke, S., Weng, Q., 2011. Per-pixel vs. object-based classification of urban land cover extraction using high spatial resolution imagery. *Remote Sens. Environ.* 115, 1145–1161.
- Myneni, R.B., Keeling, C., Tucker, C.J., Asrar, G., Nemani, R.R., 1997. Increased plant growth in the northern high latitudes from 1981 to 1991. *Nature* 386, 698–702.
- Orellana, F., Verma, P., Loheide, S.P., Daly, E., 2012. Monitoring and modeling water-vegetation interactions in groundwater-dependent ecosystems. *Rev. Geophys.* 50.
- Parent, J.R., Volin, J.C., Civco, D.L., 2015. A fully-automated approach to land cover mapping with airborne LiDAR and high resolution multispectral imagery in a forested suburban landscape. *ISPRS J. Photogramm. Remote Sens.* 104, 18–29.
- Padwick, C., Deskevich, M., Pacifici, F., Smallwood, S., 2010. WorldView-2 pan-sharpening. In: *Proceedings of the ASPRS 2010 Annual Conference*. San Diego, CA, USA.
- Pickett, S.T.A., Cadenasso, M.L., Grove, J.M., Boone, C.G., Groffman, P.M., Irwin, E., et al., 2011. Urban ecological systems: foundations and a decade of progress. *J. Environ. Manage.* 92 (3), 331–362.
- Pu, R., Landry, S., 2012. A comparative analysis of high spatial resolution IKONOS and WorldView-2 imagery for mapping urban tree species. *Remote Sens. Environ.* 124, 516–533.
- Pu, R., Landry, S., Yu, Q., 2011. Object-based urban detailed land cover classification with high spatial resolution IKONOS imagery. *Int. J. Remote Sens.* 32, 3285–3308.
- Puissant, A., Rougier, S., Stumpf, A., 2014. Object-oriented mapping of urban trees using Random Forest classifiers. *Int. J. Appl. Earth Observ. Geoinform.* 26, 235–245.
- Qian, Y., Zhou, W., Yu, W., Pickett, S.T.A., 2015. Quantifying spatiotemporal pattern of urban greenspace: new insights from high resolution data. *Landscape Ecol.* 30, 1165–1173.
- Rapinel, S., Clement, B., Magnanon, S., Sellin, V., Hubert-Moy, L., 2014. Identification and mapping of natural vegetation on a coastal site using a Worldview-2 satellite image. *J. Environ. Manage.* 144, 236–246.
- Reed, B.C., Schwartz, M.D., Xiao, X., 2009. Remote sensing phenology. *Phenology of Ecosystem Processes*. Springer, pp. 231–246.
- Richardson, A.D., Keenan, T.F., Migliavacca, M., Ryu, Y., Sonnentag, O., Toomey, M., 2013. Climate change, phenology, and phenological control of vegetation feedbacks to the climate system. *Agric. Forest Meteorol.* 169, 156–173.
- Running, S.W., Loveland, T.R., Pierce, L.L., Nemani, R., Hunt, E.R., 1995. A remote-sensing based vegetation classification logic for global land-cover analysis. *Remote Sens. Environ.* 51, 39–48.
- Sakamoto, T., Wardlow, B.D., Gitelson, A.A., Verma, S.B., Suyker, A.E., Arkebauer, T.J., 2010. A two-step filtering approach for detecting maize and soybean phenology with time-series MODIS data. *Remote Sens. Environ.* 114, 2146–2159.
- Schwartz, M.D., Reed, B.C., 1999. Surface phenology and satellite sensor-derived onset of greenness: an initial comparison. *Int. J. Remote Sens.* 20, 3451–3457.
- Schwarz, N., Schlink, U., Franck, U., Großmann, K., 2012. Relationship of land surface and air temperatures and its implications for quantifying urban heat island indicators—an application for the city of Leipzig, Germany. *Ecol. Indic.* 18, 693–704.
- Senf, C., Leitão, P.J., Pflugmacher, D., van der Linden, S., Hostert, P., 2015. Mapping land cover in complex Mediterranean landscapes using Landsat: improved classification accuracies from integrating multi-seasonal and synthetic imagery. *Remote Sens. Environ.* 156, 527–536.
- Sridharan, H., Qiu, F., 2013. Developing an object-based hyperspatial image classifier with a case study using WorldView-2 data. *Photogramm. Eng. Remote Sens.* 11, 1027–1036.
- Tigges, J., Lakes, T., Hostert, P., 2013. Urban vegetation classification: benefits of multi-temporal RapidEye satellite data. *Remote Sens. Environ.* 136, 66–75.
- Tooke, T.R., Coops, N.C., Goodwin, N.R., Voogt, J.A., 2009. Extracting urban vegetation characteristics using spectral mixture analysis and decision tree classifications. *Remote Sens. Environ.* 113, 398–407.
- Walker, J.S., Blaschke, T., 2008. Object-based land-cover classification for the Phoenix metropolitan area: optimization vs. transportability. *Int. J. Remote Sens.* 29, 2021–2040.
- White, M.A., Thornton, P.E., Running, S.W., 1997. A continental phenology model for monitoring vegetation responses to interannual climatic variability. *Glob. Biogeochem. Cycle* 11, 217–234.
- Wolter, P.T., Mladneoff, D.J., Host, G.E., Crow, T.R., 1995. Improved forest classification in the Northern Lake States using multi-temporal Landsat imagery. *Photogramm. Eng. Remote Sens.* 61, 1129–1143.
- Wu, J., Cheng, S., Li, Z., Guo, W., Zhong, F., Yin, D., 2013. Case study on rehabilitation of a polluted urban water body in Yangtze River Basin. *Environ. Sci. Pollut. Res.* 20, 7038–7045.
- Xie, S., Liu, Z., Chen, T., Hua, L., 2008. Spatiotemporal variations of ambient PM10 source contributions in Beijing in 2004 using positive matrix factorization. *Atmos. Chem. Phys.* 8, 2701–2716.
- Yan, E., Wang, G., Lin, H., Xia, C., Sun, H., 2015a. Phenology-based classification of vegetation cover types in Northeast China using MODIS NDVI and EVI time series. *Int. J. Remote Sens.* 36, 489–512.
- Yan, W., Shaker, A., El-Ashmawy, N., 2015b. Urban land cover classification using airborne LiDAR data: a review. *Remote Sens. Environ.* 158, 295–310.
- Yan, J., Lin, L., Zhou, W., Han, L., Ma, K., 2016a. Quantifying the characteristics of particulate matters captured by urban plants using an automatic approach. *J. Environ. Sci.* 39, 259–267.
- Yan, J., Lin, L., Zhou, W., Ma, K., Pickett, S.T.A., 2016b. A novel approach for quantifying particulate matter distribution on leaf surface by combining SEM and object-based image analysis. *Remote Sens. Environ.* 173, 156–161.
- Yuhendra, Alimuddin, I., Sumantyo, J.T.S., Kuze, H., 2012. Assessment of pan-sharpening methods applied to image fusion of remotely sensed multi-band data. *Int. J. Appl. Earth Observ. Geoinform.* 18, 165–175.
- Zhang, X., Friedl, M.A., Schaaf, C.B., Strahler, A.H., Hodges, J.C., Gao, F., Reed, B.C., Huete, A., 2003. Monitoring vegetation phenology using MODIS. *Remote Sens. Environ.* 84, 471–475.
- Zhang, X., Feng, X., Jiang, H., 2010. Object-oriented method for urban vegetation mapping using IKONOS imagery. *Int. J. Remote Sens.* 31, 177–196.
- Zhou, Y., Qiu, F., 2015. Fusion of high spatial resolution WorldView-2 imagery and LiDAR pseudo-waveform for object-based image analysis. *ISPRS J. Photogramm. Remote Sens.* 101, 221–232.
- Zhou, W., Troy, A., 2008. An object-oriented approach for analysing and characterizing urban landscape at the parcel level. *Int. J. Remote Sens.* 29, 3119–3135.
- Zhou, W., Huang, G., Troy, A., Cadenasso, M.L., 2009. Object-based land cover classification of shaded areas in high spatial resolution imagery of urban areas: a comparison study. *Remote Sens. Environ.* 113, 1769–1777.
- Zhou, W., Huang, G., Cadenasso, M.L., 2011. Does spatial configuration matter? Understanding the effects of land cover pattern on land surface temperature in urban landscapes. *Landscape Urban Plan.* 102, 54–63.
- Zhou, W., Pickett, S.T.A., Cadenasso, M.L., 2017a. Shifting concepts of urban spatial heterogeneity and their implications for sustainability. *Landscape Ecol.* 32 (1), 15–30.
- Zhou, W., Wang, J., Cadenasso, M.L., 2017b. Effects of the spatial configuration of trees on urban heat mitigation: a comparative study. *Remote Sens. Environ.* 195, 1–12.

Further reading

- Wu, C., Gonsamo, A., Gough, C.M., Chen, J.M., Xu, S., 2014. Modeling growing season phenology in North American forests using seasonal mean vegetation indices from MODIS. *Remote Sens. Environ.* 147, 79–88.
- Wu, C., Hou, X., Peng, D., Gonsamo, A., Xu, S., 2016. Land surface phenology of China's temperate ecosystems over 1999–2013: spatial-temporal patterns, interaction effects, covariation with climate and implications for productivity. *Agri. and For. Meteorol.* 216, 177–187.